

High-temperature topological superconductivity in twisted double layer copper oxides

Oguzhan Can, Tarun Tummuru, Ryan P. Day, Ilya Elfimov, Andrea Damascelli, and Marcel Franz
Department of Physics and Astronomy, University of British Columbia, Vancouver BC, Canada V6T 1Z4 and
Quantum Matter Institute, University of British Columbia, Vancouver BC, Canada V6T 1Z4

(Dated: December 3, 2020)

A great variety of novel phenomena occur when two-dimensional materials, such as graphene or transition metal dichalcogenides, are assembled into bilayers with a twist between individual layers. As a new application of this paradigm, we consider structures composed of two monolayer-thin d -wave superconductors with a twist angle θ that can be realized by mechanically exfoliating van der Waals-bonded high- T_c copper oxide materials, such as $\text{Bi}_2\text{Sr}_2\text{CaCu}_2\text{O}_{8+\delta}$. On the basis of symmetry arguments and detailed microscopic modelling, we predict that for a range of twist angles in the vicinity of 45° , such bilayers form a robust, fully gapped topological phase with spontaneously broken time-reversal symmetry and protected chiral Majorana edge modes. When $\theta \approx 45^\circ$, the topological phase sets in at temperatures close to the bulk $T_c \simeq 90$ K, thus furnishing a long sought realization of a true high-temperature topological superconductor.

In a remarkable recent development Yu and co-workers [1] succeeded in isolating and probing single monolayer samples of high-temperature superconductor $\text{Bi}_2\text{Sr}_2\text{CaCu}_2\text{O}_{8+\delta}$ (Bi2212) with critical temperatures T_c essentially indistinguishable from the bulk $T_c \simeq 90$ K of optimally doped Bi2212 crystals. This result delivers the long-awaited proof that high- T_c superconductivity in Bi2212 (and possibly all the cuprates) is an intrinsic property of a single two-dimensional monolayer. It also opens exciting new possibilities for engineering structures with novel behaviour and functionality, from individual high- T_c cuprate monolayers. Motivated by the results of Ref. [1] and recent developments in van der Waals-bonded materials [2–7], we consider here structures composed of two cuprate monolayers with a twist angle θ between them.

Twisted double layer graphene famously exhibits a sequence of gate-voltage controlled correlated insulating and superconducting phases [2–6] when θ is close to the magic angle 1.1° . Similar physics is reported [7] in twisted bilayer WSe₂ in the range of angles between 4.0° and 5.1° . In both cases, the observed behaviour is thought to reflect a subtle interplay between the band structure energetics and topology brought about by the Moiré patterns, electron-electron interactions and disorder [8–17]. As such, many aspects of the reported experimental observations in twisted graphene and WSe₂ still await full theoretical understanding [18]. As we argue below, the problem of twisted Bi2212 bilayers is potentially simpler to analyze theoretically, at least at the level where each Bi2212 layer is treated as a BCS superconductor with a $d_{x^2-y^2}$ order parameter. Results of such a theoretical analysis are, nevertheless, non-trivial: over a continuous range of twist angles θ in the vicinity of 45° , we find that below a critical temperature $\tilde{T}_c(\theta)$ the bilayer system spontaneously breaks time-reversal symmetry \mathcal{T} and forms a chiral topological phase that can be thought of as an emergent $d_{x^2-y^2} \pm id_{xy}$ superconductor ($d \pm id'$ for short). Such a superconductor has a

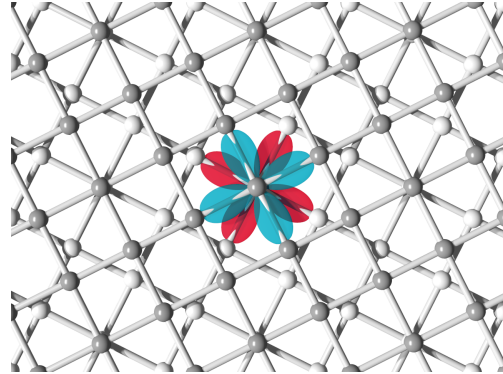


FIG. 1. Schematic view of two copper-oxygen square lattices with twist angle close to 45° . Superconducting order parameter with a $d_{x^2-y^2}$ symmetry in the twisted layer (red) resembles a d_{xy} order parameter in the original untwisted coordinate frame (blue). Although each Bi2212 monolayer contains two CuO₂ planes, for simplicity and concreteness we primarily focus on models with a single CuO₂ plane per monolayer, as would be the case in $\text{Bi}_2\text{Sr}_2\text{CuO}_{6+\delta}$ and other high- T_c compounds.

fully gapped bulk and is characterized by Chern number $C = \pm 2$ per layer with a gap of $d_{x^2-y^2} \pm id_{xy}$ symmetry, respectively. It exhibits two gapless, topologically protected chiral edge modes per monolayer. These modes are coherent superpositions of electron and hole states and can be therefore classified as Majorana particles [19]. When $\theta \approx 45^\circ$, our results indicate that $\tilde{T}_c \simeq T_c$, suggesting that, remarkably, in carefully assembled Bi2212 samples, the topological phase could set in well above the liquid nitrogen temperature.

The physics underlying the formation of the $d \pm id'$ topological phase is illustrated in Fig. 1. In momentum space, the $d_{x^2-y^2}$ order parameter that characterizes each monolayer can be represented as $\Delta_{\mathbf{k}} = \Delta_0(\hat{k}_x^2 - \hat{k}_y^2)$, where Δ_0 denotes the amplitude and $(\hat{k}_x, \hat{k}_y) = (k_x, k_y)/k$ are momentum components defined relative to the principal crystal axes of the underlying copper-

oxygen lattice. When one of the layers is rotated by angle θ , its order parameter is transformed in the original coordinate frame to

$$\Delta_{\mathbf{k}}^{(\theta)} = \Delta_0 \left[\cos(2\theta)(\hat{k}_x^2 - \hat{k}_y^2) + \sin(2\theta)2\hat{k}_x\hat{k}_y \right]. \quad (1)$$

From the vantage point of the unrotated monolayer, the second term in Eq. (1) has the functional form of a d_{xy} order parameter. For coupled layers, we then expect the Cooper pair tunneling to induce a subdominant d_{xy} order parameter in the unrotated layer. By symmetry, the same should happen in the other layer. Furthermore, if the two order parameters combine with a complex phase, the result is a fully gapped topological superconductor with broken \mathcal{T} . The gapped nature of the phase follows from the fact that the excitation gap is given by $|\Delta_{\mathbf{k}}|$ which, for a $d \pm id'$ gap function, is non-vanishing everywhere at the Fermi level, Fig. 2(a,b). \mathcal{T} -breaking is evident because time reversal maps $d + id'$ to $d - id'$. We demonstrate below that for a range of twist angles θ between θ_c^- and θ_c^+ , such a \mathcal{T} -broken phase becomes energetically favorable below a critical temperature $\tilde{T}_c(\theta)$.

We note that \mathcal{T} -broken $d \pm id'$ and $d \pm is$ phases have been discussed theoretically in various contexts, including bulk high- T_c cuprates in applied magnetic field [20–22], c -axis twist Josephson junctions [23–26], and highly doped single-layer graphene [27, 28]. However, conclusive experimental evidence for these states has never been reported. A \mathcal{T} -broken topological phase with $p_x \pm ip_y$ symmetry has long been a leading candidate for superconducting order in Sr_2RuO_4 [29–31]. Recent Knight shift measurements [32], however, appear to rule out this possibility. By placing our emphasis on monolayer-thin samples of an established $d_{x^2-y^2}$ superconductor, we argue that the present work promises to finally break the logjam in the quest for a chiral topological phase. As we show below, for $\simeq 45^\circ$ twist, the \mathcal{T} -breaking $d \pm id'$ phase is nucleated robustly and reliably through the simple and well understood mechanism of interlayer Cooper pair tunneling that is largely insensitive to microscopic details.

GINZBURG-LANDAU THEORY

The phenomenon outlined above is most easily quantified by examining the phenomenological Ginzburg-Landau (GL) theory. For the sake of clarity and simplicity, we begin by considering models with a single CuO_2 plane per monolayer. This is directly relevant to $\text{Bi}_2\text{Sr}_2\text{CuO}_{6+\delta}$ (Bi2201), but, as we show in the subsequent sections, our results are broadly applicable to cuprates with multiple CuO_2 plane structure, such as Bi2212, which has already been exfoliated [1] to the monolayer limit.

The GL free energy density for two coupled monolayers can be written as

$$\mathcal{F}[\psi_1, \psi_2] = f_0[\psi_1] + f_0[\psi_2] + A|\psi_1|^2|\psi_2|^2 + B(\psi_1\psi_2^* + \text{c.c.}) + C(\psi_1^2\psi_2^{*2} + \text{c.c.}), \quad (2)$$

where $\psi_{a=1,2}$ are complex order parameters of the two layers and $f_0[\psi] = \alpha|\psi|^2 + \frac{1}{2}\beta|\psi|^4$ is the free energy of a monolayer. We are interested in spatially uniform solutions, so the gradient terms have been omitted. If the two layers are physically identical, then the order parameter amplitudes must be the same and the most general solution (up to an overall phase) is

$$\psi_1 = \psi, \quad \psi_2 = \psi e^{i\varphi}, \quad (3)$$

where we take ψ to be real and positive.

Because ψ_a describe order parameters with d -wave symmetry, they transform as $\psi_a \rightarrow -\psi_a$ under a 90° rotation. Suppose we increase the twist angle θ continuously from 0 to $\pi/2$. Since ψ_2 changes sign under this operation, we conclude that for the free energy (2) to remain invariant, the parameter B must also change sign. The simplest dependence consistent with this constraint is $B = -B_0 \cos(2\theta)$, where we take $B_0 > 0$. The negative sign is chosen to allow the phase difference between the layers to vanish as the twist angle approaches zero. This also implies that $B = 0$ for $\theta = \pi/4$, consistent with the intuition that a $d_{x^2-y^2}$ Cooper pair cannot tunnel between the layers in this configuration. Parameters A and C are not required by symmetry to depend on θ , so we treat them as constants henceforth. Incorporating these ingredients into Eq. (2), we find

$$\mathcal{F}(\varphi) = \mathcal{F}_0 + 2B_0\psi^2[-\cos(2\theta)\cos\varphi + \mathcal{K}\cos(2\varphi)], \quad (4)$$

where $\mathcal{K} = C\psi^2/B_0$ and \mathcal{F}_0 contains all terms independent of φ . It is now a simple matter to minimize $\mathcal{F}(\varphi)$ for a given twist angle θ . An interesting scenario arises when $\mathcal{K} > 0$, as indicated by Fig. 2(c). Although symmetry alone does not constrain the sign of \mathcal{K} , a simple physical argument suggests that \mathcal{K} should, in general, be positive. One can interpret the $\psi_1^2\psi_2^{*2}$ term in Eq. (2) as representing the coherent tunneling of *two* Cooper pairs between the layers. Up to an overall scale factor, its coefficient should, therefore, be proportional to the square of the coefficient B , which itself corresponds to single pair tunneling. Coefficient C (and, hence, also \mathcal{K}) will then be positive, regardless of the sign of B . Below, we demonstrate that microscopic models fully support this argument, yielding $\mathcal{K} > 0$.

At $\theta = 45^\circ$ and for $\mathcal{K} > 0$, the free energy minimum clearly occurs at $\varphi_{\min} = \pm\pi/2$ which indicates a $d \pm id'$ superconducting state. For $\theta \neq 45^\circ$, the free energy is minimized by

$$\varphi_{\min} = \arccos\left(\frac{\cos 2\theta}{4\mathcal{K}}\right). \quad (5)$$

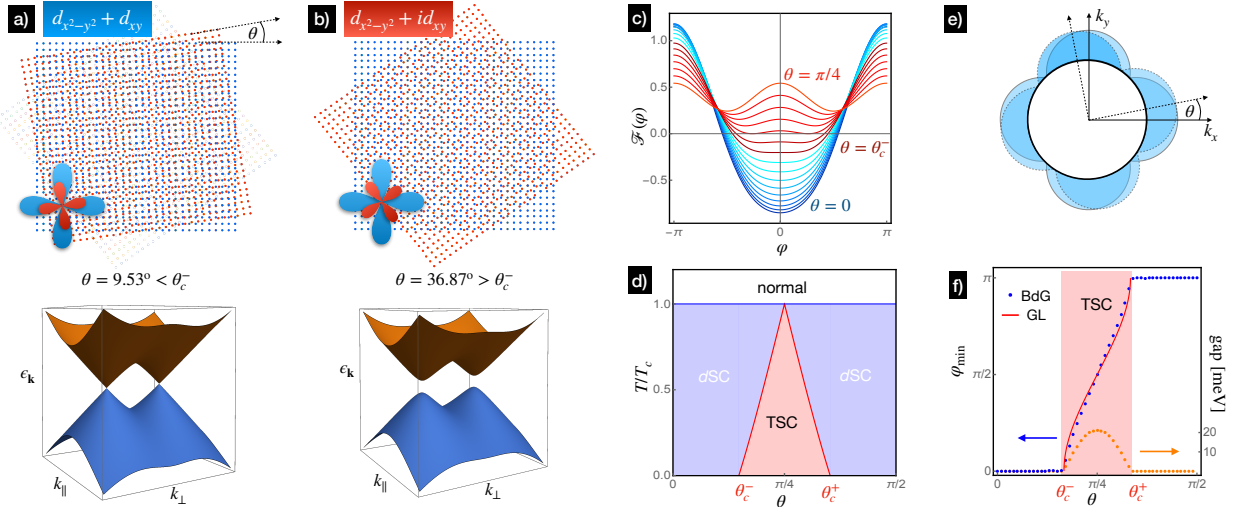


FIG. 2. Twisted double layer d -wave superconductor. Panel (a) illustrates the lattice geometry at small twist angle $\theta < \theta_c^-$ where the free energy is minimized for interlayer phase difference $\varphi = 0$. This results in a gapless spectrum with weakly split Dirac points. For twist angles $\theta > \theta_c^-$ in panel (b) the preferred state has $\varphi \neq 0$. It breaks time reversal and is fully gapped as indicated by the massive Dirac spectrum. The spectra are obtained by diagonalizing the BdG Hamiltonian (10); k_\perp and k_\parallel denote momentum components perpendicular and parallel to the Fermi surface near a nodal point. Panel (c) shows the GL free energy $\mathcal{F}(\varphi)$ for twist angles θ ranging from 0° to 45° in 3° increments for $K = 0.125$. When $\theta > \theta_c^-$ minima occur away from $\varphi = 0$. Panel (d): predicted phase diagram based on the the GL theory (2) and $\tilde{T}_c(\theta)$ given by Eq. (6). TSC denotes the gapped topological phase, d SC stands for gapless d -wave superconductor. Panel (e): Fermi surface and d -wave gap in the continuum formulation of the microscopic model. Panel (f) displays the relative phase between the layers φ_{\min} that minimizes the GL and the BdG free energy as a function of twist angle θ . Orange symbols represent the spectral gap.

As illustrated in Fig. 2(f), a nontrivial phase difference occurs for a range of angles $\theta_c^- < \theta < \theta_c^+$ with $\theta_c^\pm = \frac{1}{2} \arccos(\mp 4K)$. This indicates a \mathcal{T} -broken phase with order parameter $d_{x^2-y^2} + e^{\pm i\varphi_{\min}} d_{xy}$ which is fully gapped and topologically non-trivial as long as $\varphi_{\min} \neq 0, \pi$, see also Fig. 2(a,b). As K depends on temperature through its dependence on ψ , the critical temperature \tilde{T}_c of the topological phase will be a function of the twist angle θ . If we adopt the standard GL temperature dependence for the order parameter $\psi(T) = \psi_0 \sqrt{1 - T/T_c}$, it is straightforward to deduce

$$\tilde{T}_c(\theta) = T_c \left(1 - \frac{|\cos 2\theta|}{4K_0} \right), \quad \theta_c^- < \theta < \theta_c^+, \quad (6)$$

where $K_0 = C\psi_0^2/B_0$. This defines the phase diagram in Fig. 2(d). We observe that, remarkably, $\tilde{T}_c(45^\circ)$ coincides with the T_c of a single monolayer which can be as high as 90 K in carefully prepared Bi2212 flakes. Away from the ideal 45° twist, the critical temperature falls approximately as $\tilde{T}_c(\theta) \simeq T_c(1 - |\theta - \pi/4|/2K_0)$. Microscopic models with realistic Bi2212 parameters discussed in the following give typical values $K_0 \simeq 0.1 - 0.2$, implying a significant extent for the topological phase, as indicated in Fig. 2(d).

MICROSCOPIC MODELS

We now turn to the microscopic theory. Although the pairing mechanism in high- T_c cuprates remains a subject of debate, it is widely accepted that most physical properties of the superconducting state in the optimally doped and overdoped regime are accurately described within the framework of the standard BCS theory with a $d_{x^2-y^2}$ order parameter. Therefore, we begin by modeling the twisted bilayer using a simple continuum model of coupled d -wave superconductors, and complement this with a calculation based on an attractive Hubbard model on the square lattice. The continuum formulation has the advantage of being applicable to an arbitrary twist angle θ , similar to the Bistritzer-MacDonald model for graphene [8]. In contrast with the continuum model above, the lattice calculation captures various microscopic details of CuO₂ planes more effectively, such as the shape of the Fermi surface. It is, however, limited to commensurate twist angles that produce relatively small Moiré unit cells due to practical constraints.

In keeping with the strategy outlined above, we begin with a single CuO₂ plane per monolayer, as for Bi2201. The continuum theory for such a bilayer is defined by the

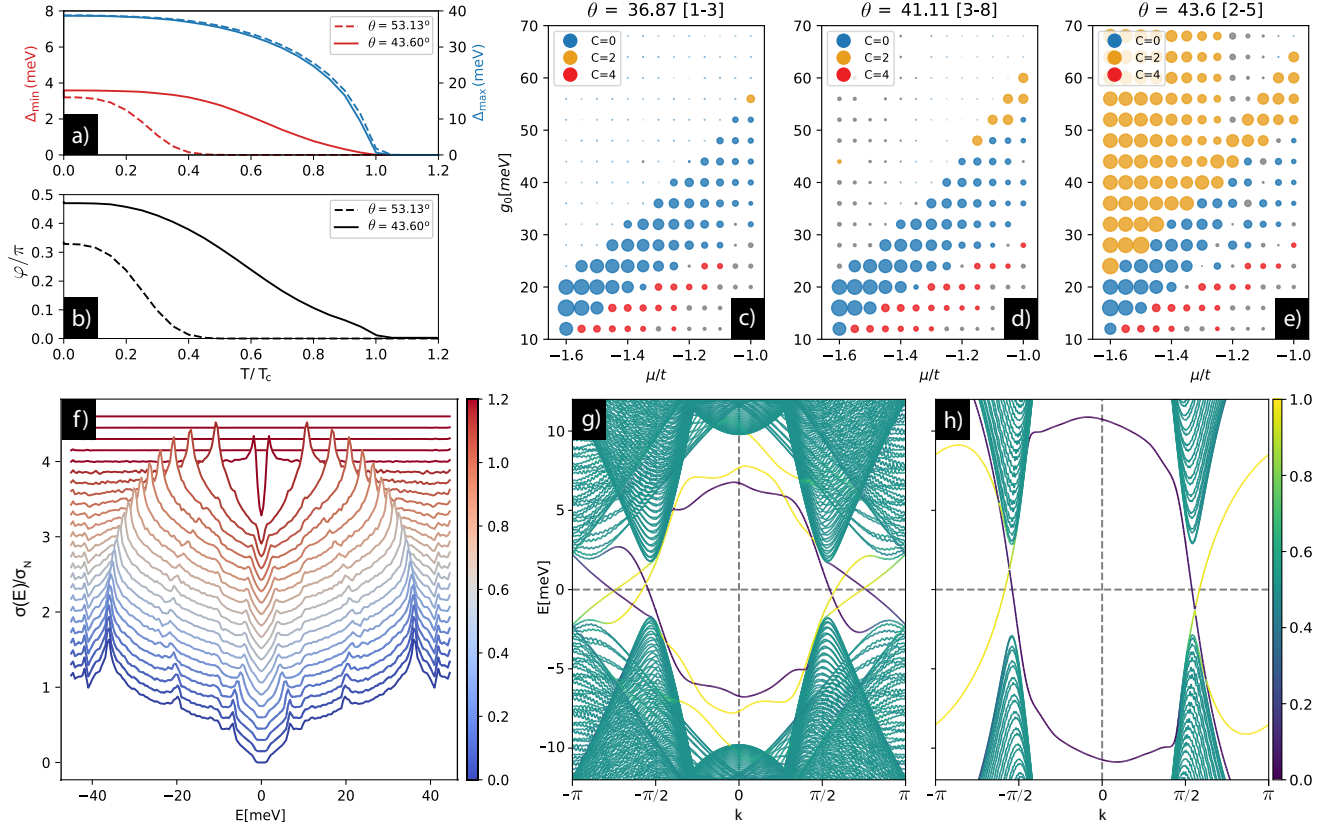


FIG. 3. Lattice model results. Panels (a,b) show the temperature dependence of the minimum gap Δ_{\min} , the maximum gap Δ_{\max} and phase φ , based on a fully self-consistent lattice calculation for coupled layers with commensurate twist angles $\theta_{1,2} \simeq 53.13^\circ$, and $\theta_{2,5} \simeq 43.60^\circ$ corresponding to a unit cell with 10 and 58 sites, respectively. Panels (c-e) show zero temperature phase diagrams of the system for three twist angles as a function of chemical potential μ and interlayer coupling g_0 . The range of chemical potentials $\mu \in (-1.6t, -1.0t)$ correspond to range of fillings $n \in (0.033, 0.04)$ near optimal doping. Each data point in the phase diagram corresponds to an independent self-consistent solution and the radius of markers is proportional to the size of the minimum gap Δ_{\min} . The color indicates the Chern number as shown in the legend. Panel (f) displays tunneling conductance $\sigma(E)/\sigma_N$ calculated for $\theta \simeq 53.13^\circ$, $\mu/t = -1.3$, $g_0 = 20$ meV and temperatures ranging from 0 to $1.2T_c$ as indicated by color scale. Curves for different temperatures have been offset for clarity. Panels (g) and (h) illustrate the edge modes for $C = 4$ and $C = 2$ topological phases, respectively, in the $\theta_{2,5}$ configuration for parameters $\mu = -1.3t$ and $g_0 = 20, 52$ meV. The energy spectrum is shown for a bilayer system in the infinite strip geometry with width of 90 unit cells. The color scale represents the normalized position expectation value of the eigenstate along the direction of finite length.

Hamiltonian

$$\mathcal{H} = \sum_{\mathbf{k}\sigma a} \xi_{\mathbf{k}a} c_{\mathbf{k}\sigma a}^\dagger c_{\mathbf{k}\sigma a} + g \sum_{\mathbf{k}\sigma} \left(c_{\mathbf{k}\sigma 1}^\dagger c_{\mathbf{k}\sigma 2} + \text{h.c.} \right) \quad (7)$$

$$+ \sum_{\mathbf{k}a} \left(\Delta_{\mathbf{k}a} c_{\mathbf{k}\uparrow a}^\dagger c_{-\mathbf{k}\downarrow a}^\dagger + \text{h.c.} \right) - \sum_{\mathbf{k}a} \Delta_{\mathbf{k}a} \langle c_{\mathbf{k}\uparrow a}^\dagger c_{-\mathbf{k}\downarrow a}^\dagger \rangle.$$

Here, $c_{\mathbf{k}\sigma a}^\dagger$ creates an electron with crystal momentum \mathbf{k} and spin σ in layer $a = 1, 2$ while $\xi_{\mathbf{k}a}$ and g represent the in-plane kinetic energy and inter-plane tunneling amplitude, respectively. The superconducting order parameter in layer a can then be expressed as

$$\Delta_{\mathbf{k}a} = \sum_{\mathbf{p}}' V_{\mathbf{k}\mathbf{p}}^{(a)} \langle c_{-\mathbf{p}\downarrow a} c_{\mathbf{p}\uparrow a} \rangle. \quad (8)$$

The prime on the summation indicates a restriction to

momentum states with energy within ϵ_c of the Fermi level. The Hamiltonian (7) should be regarded as a mean-field approximation to the BCS pairing Hamiltonian with an interaction term $\sum_{\mathbf{k}\mathbf{p}} V_{\mathbf{k}\mathbf{p}}^{(a)} c_{\mathbf{k}\uparrow a}^\dagger c_{-\mathbf{k}\downarrow a}^\dagger c_{-\mathbf{p}\downarrow a} c_{\mathbf{p}\uparrow a}$, where $V_{\mathbf{k}\mathbf{p}}^{(a)}$ denotes the interaction matrix element in layer a . We shall use a simple separable form

$$V_{\mathbf{k}\mathbf{p}}^{(a)} = -2\mathcal{V} \cos(2\alpha_{\mathbf{k}}) \cos(2\alpha_{\mathbf{p}}), \quad (9)$$

where $\alpha_{\mathbf{k}}$ represents the polar angle of the vector \mathbf{k} . This is known to yield a robust solution with $d_{x^2-y^2}$ symmetry for a single CuO_2 layer, namely $\Delta_{\mathbf{k}a} = \Delta_d \cos(2\alpha_{\mathbf{k}})$.

In order to incorporate the twist, we take the interaction in layer 1 as in Eq. (9), but we rotate the interaction in layer 2 by angle θ such that $V_{\mathbf{k}\mathbf{p}}^{(2)} = -2\mathcal{V} \cos(2\alpha_{\mathbf{k}} - 2\theta) \cos(2\alpha_{\mathbf{p}} - 2\theta)$. For the sake of sim-

plicity, we consider a circular Fermi surface generated by $\xi_{\mathbf{k}a} = \hbar^2 k^2 / 2m - \mu$ that remains invariant under rotation, see Fig. 2(e). The problem posed by Hamiltonian (7) is then solved by defining a four-component Nambu spinor $\Psi_{\mathbf{k}} = (c_{\mathbf{k}\uparrow 1}, c_{-\mathbf{k}\downarrow 1}^\dagger, c_{\mathbf{k}\uparrow 2}, c_{-\mathbf{k}\downarrow 2}^\dagger)^T$ in terms of which $\mathcal{H} = \sum_{\mathbf{k}} \Psi_{\mathbf{k}}^\dagger h_{\mathbf{k}} \Psi_{\mathbf{k}} + E_0$. Here, the Bogoliubov-de Gennes (BdG) Hamiltonian reads

$$h_{\mathbf{k}} = \begin{pmatrix} \xi_{\mathbf{k}} & \Delta_{\mathbf{k}1} & g & 0 \\ \Delta_{\mathbf{k}1}^* & -\xi_{\mathbf{k}} & 0 & -g \\ g & 0 & \xi_{\mathbf{k}} & \Delta_{\mathbf{k}2} \\ 0 & -g & \Delta_{\mathbf{k}2}^* & -\xi_{\mathbf{k}} \end{pmatrix} \quad (10)$$

and $E_0 = \sum_{\mathbf{k}} 2\xi_{\mathbf{k}} - \sum_{\mathbf{k}a} \Delta_{\mathbf{k}a} (c_{\mathbf{k}\uparrow a}^\dagger c_{-\mathbf{k}\downarrow a})$. Diagonalizing $h_{\mathbf{k}}$ gives two pairs of energy eigenvalues $\pm E_{\mathbf{k}\alpha}$ ($\alpha = 1, 2$) for each momentum \mathbf{k} . With the Hamiltonian (7) expressed in diagonal form, the free energy of the system can be calculated from the standard expression

$$\mathcal{F}_{\text{BdG}} = E_0 - 2k_B T \sum_{\mathbf{k}\alpha} \ln [2 \cosh (E_{\mathbf{k}\alpha} / 2k_B T)]. \quad (11)$$

By performing a systematic expansion of \mathcal{F}_{BdG} in powers of the order parameter amplitudes Δ_d , it is possible to ascertain various coefficients entering the GL free energy (2). This confirms the form of the GL coefficients B and C deduced previously on the basis of general symmetry arguments, and that \mathcal{K} in Eq. (4) is positive. This calculation is summarized in Methods.

We proceed with a fully self-consistent solution which follows from minimizing \mathcal{F}_{BdG} with respect to $\Delta_{\mathbf{k}a}$ and can be performed for any given \mathcal{V} , twist angle θ and temperature T . To facilitate this calculation we assume that the order parameters in the two layers have the same amplitude Δ_d , but can differ in phase as in Eq. (3). Free energy computed from Eq. (11) then shows the same qualitative behaviour as the GL theory (4) with $\mathcal{K} > 0$: for small twist angles, $\mathcal{F}_{\text{BdG}}(\varphi)$ has a single minimum at $\varphi = 0$, while for twist angles close to 45° there are always two degenerate minima at $\varphi = \pm\varphi_{\min}$, indicating formation of a \mathcal{T} -broken topological phase. Fig. 2(f) shows the calculated φ_{\min} as a function of the twist angle θ for realistic Bi2212 parameters [33–35] $\Delta_d = 40$ meV, $g = 30$ meV, $\epsilon_c = 60$ meV at $T = 0$. We observe an excellent agreement with the prediction of the GL theory when $\mathcal{K} = 0.125$. The BdG theory also allows us to predict the minimum excitation gap which, in this simple model, can be as large as 20 meV when θ is close to 45° .

The BdG theory can be formulated directly on the lattice by starting from the Hubbard model with on-site repulsion and nearest-neighbour attraction. This is known to produce a $d_{x^2-y^2}$ superconductor when applied to a single CuO₂ monolayer. The Hamiltonian is

$$\begin{aligned} H = & - \sum_{ij,\sigma a} t_{ij} c_{i\sigma a}^\dagger c_{j\sigma a} - \mu \sum_{i\sigma a} n_{i\sigma a} \\ & + \sum_{ij,a} V_{ij} n_{ia} n_{ja} - \sum_{ij\sigma} g_{ij} c_{i\sigma 1}^\dagger c_{j\sigma 2}, \end{aligned} \quad (12)$$

where t_{ij} encodes the normal-state band structure of the single layer, g_{ij} describes the interlayer tunneling and V_{ij} denotes density-density interactions. The mean-field calculations are performed in bilayer geometries characterized by a twist vector $\mathbf{v} = (m, n)$ and commensurate twist angle $\theta_{m,n} = 2 \arctan(m/n)$ as explained in Methods. Fig. 3 summarizes our main results. These lend further support to our conclusions drawn on the basis of the GL and continuum BdG approaches and show additional interesting features.

The lattice model confirms the onset of the \mathcal{T} -breaking phase below critical temperature $\tilde{T}_c(\theta)$ whose dependence on θ is consistent with the GL prediction, see Fig. 3(a,b). The results are in reasonable quantitative agreement with the continuum BdG theory but the lattice model gives a smaller spectral gap. This may be attributed to more complicated Fermi surface geometry resulting from Brillouin zone folding that accompanies the large real-space Moiré unit cell. The lattice model allows for a direct evaluation of the Chern number C , as discussed in Methods. In addition to the $C = 4$ topological phase anticipated on the basis of the continuum BdG theory, the $T = 0$ phase diagrams in Fig. 3(c-e) reveal the existence of $C = 2$ and $C = 0$ gapped phases that can be reached by varying the chemical potential μ and the interlayer coupling strength g_0 . In an experiment, the former can be tuned over a wide range by oxygen annealing [1], while the latter may depend on the twist angle θ and could be further controlled by applying hydrostatic pressure as demonstrated in twisted graphene [4]. As explained in Methods, the $C = 0$ phase corresponds to a $d + is$ superconductor, while the $C = 2$ phase can be effectively thought of as a single-layer $d + id'$ superconductor. For a strip geometry, the lattice model predicts protected chiral edge modes traversing the bulk gap, Fig. 3(g,h), confirming the topological nature of the $d + id'$ phase.

Additional interesting behaviour is observed at nonzero temperature. Fig. 10 in Methods shows a phase transition from $d + is$ to $d + id$ phase driven by increasing T . As we discuss in more detail below, all these phenomena are experimentally accessible using standard spectroscopic, thermodynamic and transport techniques.

STABILITY ANALYSIS AND THE DENSITY FUNCTIONAL THEORY

In order to establish the physical stability of the twisted double layer structure and to estimate the interlayer coupling, we performed extensive Density Functional Theory (DFT) simulations. We have employed the structure of Bi2201; with a single CuO₂ plane per monolayer, it has a direct connection to the $N = 1$ layer continuum and lattice models. Furthermore, the volume of the unit cell is greatly reduced with respect to Bi2212, facilitating calculation of the freestanding bilayer heterostruc-

ture. This analysis is focused on the coupling between two CuO₂ blocks; as for the previous section, we do not expect the additional internal structure of each block in the $N > 1$ case to change our results substantively.

Bi2201 supercells in the $\mathbf{v} = (1, 2)$ geometry were constructed from a bulk model defined with an in-plane Cu-Cu distance of $a = 3.99 \text{ \AA}$, and unit-cell height of $c = 23.98 \text{ \AA}$. The tetragonal $I4/mmm$ space group was imposed to minimize complications due to the small orthorhombicity of the actual material. Two unit cells, each containing a single CuO₂ plane and counter-rotated by the twist angle were combined in a freestanding bilayer construction, with a vacuum buffer of 15\AA, see Fig. 4(a). We considered two high-symmetry configurations of the bilayer unit cell, with the two layers translated by (0,0) and $(\sqrt{5}a/2, \sqrt{5}a/2)$, as illustrated in Fig. 4(b,c). The Kohn-Sham equations were solved self-consistently using the SCAN meta-GGA exchange correlation potential [36], as implemented in VASP [37, 38]. As opposed to standard GGA, the recently developed SCAN functional incorporates kinetic-energy corrections, supporting the study of mixed-bonding environments [36]. In bilayer cuprates, weak van der Waals and ionic bonding coexist, making this approach well-suited to the problem [39, 40]. This circumvents the need for empirical van der Waals corrections to the GGA. We repeated this process for various inter-bilayer distances to ascertain the energetic stability of the bilayer compound. In the inset of panel (d), we plot the total ground state energy, evaluated relative to the limit of two independent monolayers. In both translational configurations, we find a similar energy minimum near 12.87 \AA. We note that this is the distance between neighbouring CuO₂ layers; the BiO layers which constitute the bilayer interface are 9.45 \AA closer together. These results are largely independent of the exchange correlation potential used, as explored in Methods.

To estimate the strength of interlayer coupling between neighbouring CuO₂ layers, we identify an avoided crossing at the X point of the Bi2201 Brillouin zone, indicated in the bandstructure of Fig. 4(e). The size of this splitting decays with the Cu-Cu distance, to a value of ~ 5 meV at the optimal spacing of 12.87 \AA, as shown in Fig. 4(d). We emphasize that this splitting does not provide a direct measure of the parameter g_0 , but establishes evidence for finite Cu-Cu interlayer coupling within the energy scale surveyed in the text. It is important to note that there is precedent for a renormalization of the DFT-derived interlayer coupling strength in cuprates, as measured via photoemission. These renormalization factors vary over a range of at least 2-5 in different materials [41]. Additional details of the calculations presented here can be found in the Methods section.

OUTLOOK

Our results establish a new avenue for engineering high-temperature topological superconductors by combining monolayers of van der Waals-bonded d -wave superconducting cuprates, such as Bi₂Sr₂CuO_{6+δ} or Bi₂Sr₂CaCu₂O_{8+δ} [1]. The topological phase is fully gapped, breaks time reversal symmetry and supports protected chiral Majorana modes at the sample boundary. The chiral $d \pm id'$ phase arises robustly, driven by Cooper pair tunneling between the layers when they are twisted by an angle close to 45°. Unlike in graphene, where the twist angle must be tuned very accurately, we predict that a wide range of angles ($45^\circ \pm 10^\circ$) will produce non-trivial physics in these systems.

The resulting fully gapped topological phase can be probed by conventional spectroscopic or transport techniques. For example, on lowering the sample temperature, angle resolved photoemission or tunneling spectroscopies [34, 35] will detect the transition at $T = \tilde{T}_c(\theta)$ from the gapless $d_{x^2-y^2}$ superconductor with Dirac nodes to a fully gapped excitation spectrum. This change should also be observable via thermodynamic probes such as those measuring the specific heat [42] and superfluid density [43, 44]. Signatures of the broken \mathcal{T} -symmetry characteristic of the $d \pm id'$ and $d + is$ phases may be identified by circular birefringence and dichroism experiments [45]. In transport, the non-zero Chern number manifests as quantized electronic contribution to the thermal Hall conductance $\kappa_{xy} = C(\pi^2 k_B^2 T / 3h)$ [22]. In mesoscopic samples, longitudinal thermal conductance κ_{xx} will also be quantized due to the ballistic contribution of the edge states. The $d \pm id'$ phase exhibits anomalous interlayer Josephson effect due to the two-minima structure of the free energy depicted in Fig. 2(c); the Josephson current $I_J = (2e/h)\partial\mathcal{F}/\partial\varphi$ will develop pronounced deviations from the usual sinusoidal dependence on the phase bias $\Delta\varphi = \varphi - \varphi_{\min}$.

It is worth noting that existing experimental results on c -axis twist Josephson tunneling in cuprates already offer some support for the ideas advanced here. According to symmetry analysis, which assumes unbroken time reversal and pure $d_{x^2-y^2}$ order parameter, the Josephson current I_J must vanish when $\theta = 45^\circ$ [23–25]. In Methods, we show that for a $d + id'$ state I_J , however, remains nonzero at $\theta = 45^\circ$. Non-vanishing I_J has often been interpreted as evidence for conventional s -wave order parameter in experiments [46, 47]. Given what we know about the order parameter symmetry in cuprates today, one may argue that a more plausible explanation for non-vanishing I_J is the spontaneously \mathcal{T} -broken phase advocated in this work.

The authors are indebted to D.A. Bonn, D.M. Broun, J.A. Folk, C. Kallin, C. Li, É. Lantagne-Hurtubise, S. Plugge, S. Sahoo, O. Vafek and Z. Ye for valuable dis-

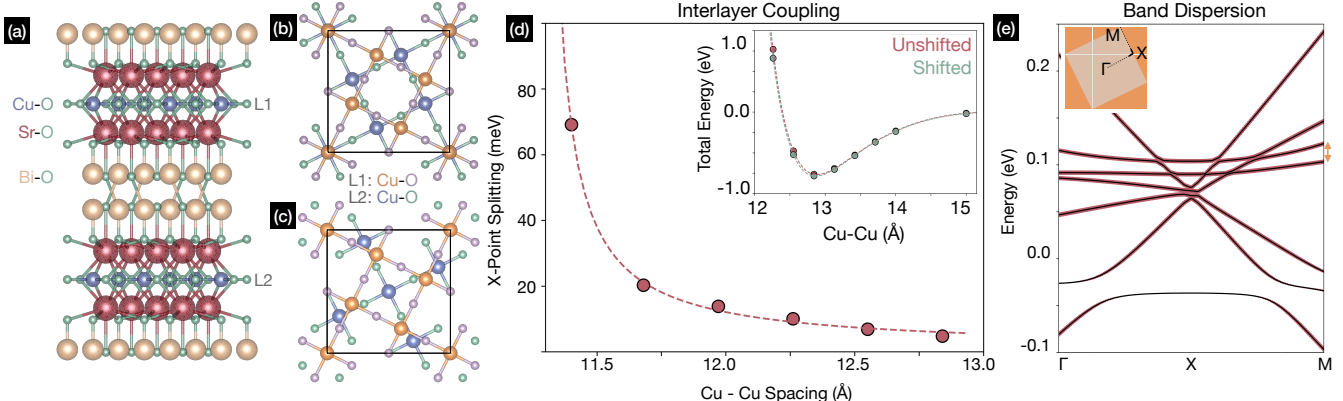


FIG. 4. Crystal structure and results of the twisted double layer DFT calculations. In panel (a), side view of the unit cell with unshifted monolayers. Top view of the CuO₂ planes are illustrated for the unshifted (b) and shifted (c) unit cells. For the unit cell in (b), we plot the splitting at the X point as a function of the Cu - Cu distance in (d). A narrow window of the twisted bilayer bandstructure near the X point of the original Bi2201 Brillouin zone is provided in (e), at a Cu-Cu spacing of 11.97 Å. The pair of bands used for defining the splitting in (d) are identified by the orange arrow. A fit of the X -point splitting to $1/x$ is shown as a dashed red line in (d). The equilibrium layer spacing is solved for as the minimum in the system's total energy, as illustrated by the inset. The total energy of the bilayer unit cell is given for both unit cells in (b,c). The energy scale is defined relative to the limit of two isolated monolayers.

cussions and correspondence. The work described here was supported by NSERC. This research was undertaken thanks in part to funding from the Max Planck-UBC-UTokyo Centre for Quantum Materials and the Canada First Research Excellence Fund, Quantum Materials and Future Technologies Program. OC is supported by International Doctoral Fellowship from UBC.

Data availability

This manuscript contains no experimental data.

Code availability

The complete code used to obtain results shown in Fig. 3 will be made publicly available at <https://github.com/oceanphys/tbcuprate/>. DFT results shown in Fig. 4 were obtained VASP [37, 38]. Input files are also available through our repository.

in magic-angle graphene superlattices, *Nature (London)* **556**, 80 (2018).

- [3] Y. Cao, V. Fatemi, S. Fang, K. Watanabe, T. Taniguchi, E. Kaxiras, and P. Jarillo-Herrero, Unconventional superconductivity in magic-angle graphene superlattices, *Nature (London)* **556**, 43 (2018).
- [4] M. Yankowitz, S. Chen, H. Polshyn, Y. Zhang, K. Watanabe, T. Taniguchi, D. Graf, A. F. Young, and C. R. Dean, Tuning superconductivity in twisted bilayer graphene, *Science* **363**, 1059 (2019).
- [5] A. L. Sharpe, E. J. Fox, A. W. Barnard, J. Finney, K. Watanabe, T. Taniguchi, M. A. Kastner, and D. Goldhaber-Gordon, Emergent ferromagnetism near three-quarters filling in twisted bilayer graphene, *Science* **365**, 605 (2019).
- [6] X. Lu, P. Stepanov, W. Yang, M. Xie, M. A. Aamir, I. Das, C. Urgell, K. Watanabe, T. Taniguchi, G. Zhang, A. Bachtold, A. H. MacDonald, and D. K. Efetov, Superconductors, orbital magnets and correlated states in magic-angle bilayer graphene, *Nature* **574**, 653 (2019).
- [7] L. Wang, E.-M. Shih, A. Ghiotto, L. Xian, D. A. Rhodes, C. Tan, M. Claassen, D. M. Kennes, Y. Bai, B. Kim, K. Watanabe, T. Taniguchi, X. Zhu, J. Hone, A. Rubio, A. Pasupathy, and C. R. Dean, Magic continuum in twisted bilayer WSe₂, arXiv e-prints , arXiv:1910.12147 (2019), [arXiv:1910.12147 \[cond-mat.mes-hall\]](https://arxiv.org/abs/1910.12147).
- [8] R. Bistritzer and A. H. MacDonald, Moiré bands in twisted double-layer graphene, *Proceedings of the National Academy of Science* **108**, 12233 (2011).
- [9] N. N. T. Nam and M. Koshino, Lattice relaxation and energy band modulation in twisted bilayer graphene, *Phys. Rev. B* **96**, 075311 (2017).
- [10] J. Kang and O. Vafek, Symmetry, maximally localized wannier states, and a low-energy model for twisted bilayer graphene narrow bands, *Phys. Rev. X* **8**, 031088 (2018).

- [11] L. Zou, H. C. Po, A. Vishwanath, and T. Senthil, Band structure of twisted bilayer graphene: Emergent symmetries, commensurate approximants, and Wannier obstructions, *Phys. Rev. B* **98**, 085435 (2018).
- [12] H. C. Po, L. Zou, A. Vishwanath, and T. Senthil, Origin of mott insulating behavior and superconductivity in twisted bilayer graphene, *Phys. Rev. X* **8**, 031089 (2018).
- [13] M. Xie and A. H. MacDonald, Nature of the correlated insulator states in twisted bilayer graphene, *Phys. Rev. Lett.* **124**, 097601 (2020).
- [14] M. Koshino, N. F. Q. Yuan, T. Koretsune, M. Ochi, K. Kuroki, and L. Fu, Maximally localized wannier orbitals and the extended hubbard model for twisted bilayer graphene, *Phys. Rev. X* **8**, 031087 (2018).
- [15] F. Guinea and N. R. Walet, Electrostatic effects, band distortions, and superconductivity in twisted graphene bilayers, *Proceedings of the National Academy of Science* **115**, 13174 (2018).
- [16] J. Kang and O. Vafek, Strong Coupling Phases of Partially Filled Twisted Bilayer Graphene Narrow Bands, *Phys. Rev. Lett.* **122**, 246401 (2019).
- [17] K. Hejazi, C. Liu, H. Shapourian, X. Chen, and L. Balents, Multiple topological transitions in twisted bilayer graphene near the first magic angle, *Phys. Rev. B* **99**, 035111 (2019).
- [18] E. Y. Andrei and A. H. MacDonald, Graphene Bilayers with a Twist, arXiv e-prints , arXiv:2008.08129 (2020), arXiv:2008.08129 [cond-mat.mes-hall].
- [19] S. R. Elliott and M. Franz, Colloquium: Majorana fermions in nuclear, particle, and solid-state physics, *Rev. Mod. Phys.* **87**, 137 (2015).
- [20] R. B. Laughlin, Magnetic induction of $d_{x^2-y^2} + id_{xy}$ order in high- T_c superconductors, *Phys. Rev. Lett.* **80**, 5188 (1998).
- [21] M. Franz and Z. Tešanović, Self-consistent electronic structure of a $d_{x^2-y^2}$ and a $d_{x^2-y^2} + id_{xy}$ vortex, *Phys. Rev. Lett.* **80**, 4763 (1998).
- [22] A. Vishwanath, Quantized thermal hall effect in the mixed state of d -wave superconductors, *Phys. Rev. Lett.* **87**, 217004 (2001).
- [23] K. Kuboki and M. Sigrist, Proximity-induced time-reversal symmetry breaking at josephson junctions between unconventional superconductors, *Journal of the Physical Society of Japan* **65**, 361 (1996).
- [24] A. Bille, R. A. Klemm, and K. Scharnberg, Models of c-axis twist josephson tunneling, *Phys. Rev. B* **64**, 174507 (2001).
- [25] T. Yokoyama, S. Kawabata, T. Kato, and Y. Tanaka, Theory of macroscopic quantum tunneling in high- T_c c-axis josephson junctions, *Phys. Rev. B* **76**, 134501 (2007).
- [26] Z. Yang, S. Qin, Q. Zhang, C. Fang, and J. Hu, $\pi/2$ -josephson junction as a topological superconductor, *Phys. Rev. B* **98**, 104515 (2018).
- [27] S. Pathak, V. B. Shenoy, and G. Baskaran, Possible high-temperature superconducting state with a $d + id$ pairing symmetry in doped graphene, *Phys. Rev. B* **81**, 085431 (2010).
- [28] R. Nandkishore, L. S. Levitov, and A. V. Chubukov, Chiral superconductivity from repulsive interactions in doped graphene, *Nature Physics* **8**, 158 (2012).
- [29] T. M. Rice and M. Sigrist, Sr₂ruo4: an electronic analogue of 3he?, *Journal of Physics: Condensed Matter* **7**, L643 (1995).
- [30] K. Ishida, H. Mukuda, Y. Kitaoka, K. Asayama, Z. Q. Mao, Y. Mori, and Y. Maeno, Spin-triplet superconductivity in sr₂ruo4 identified by 17o knight shift, *Nature* **396**, 658 (1998).
- [31] C. Kallin and A. J. Berlinsky, Is sr₂ruo4a chiral p-wave superconductor?, *Journal of Physics: Condensed Matter* **21**, 164210 (2009).
- [32] A. Pustogow, Y. Luo, A. Chronister, Y. S. Su, D. A. Sokolov, F. Jerzembeck, A. P. Mackenzie, C. W. Hicks, N. Kikugawa, S. Raghu, E. D. Bauer, and S. E. Brown, Constraints on the superconducting order parameter in sr₂ruo4 from oxygen-17 nuclear magnetic resonance, *Nature* **574**, 72 (2019).
- [33] O. Andersen, A. Liechtenstein, O. Jepsen, and F. Paulsen, Lda energy bands, low-energy hamiltonians, t' , t'' , $t_\perp(k)$, and j_\perp , arXiv preprint cond-mat/9509044 (1995).
- [34] A. Damascelli, Z. Hussain, and Z.-X. Shen, Angle-resolved photoemission studies of the cuprate superconductors, *Rev. Mod. Phys.* **75**, 473 (2003).
- [35] O. Fischer, M. Kugler, I. Maggio-Aprile, C. Berthod, and C. Renner, Scanning tunneling spectroscopy of high-temperature superconductors, *Rev. Mod. Phys.* **79**, 353 (2007).
- [36] J. Sun, A. Ruzsinszky, and J. P. Perdew, Strongly constrained and appropriately normed semilocal density functional, *Phys. Rev. Lett.* **115**, 036402 (2015).
- [37] G. Kresse and J. Hafner, Ab initio molecular dynamics for open-shell transition metals, *Phys. Rev. B* **48**, 13115 (1993).
- [38] G. Kresse and J. Furthmüller, Efficient iterative schemes for ab initio total-energy calculations using a plane-wave basis set, *Phys. Rev. B* **54**, 11169 (1996).
- [39] J. W. Furness, Y. Zhang, C. Lane, I. G. Buda, B. Barbiellini, R. S. Markiewicz, A. Bansil, and J. Sun, An accurate first-principles treatment of doping-dependent electronic structure of high-temperature cuprate superconductors, *Communications Physics* **1**, 11 (2018).
- [40] Y. Zhang, C. Lane, J. W. Furness, B. Barbiellini, J. P. Perdew, R. S. Markiewicz, A. Bansil, and J. Sun, Competing stripe and magnetic phases in the cuprates from first principles, *Proceedings of the National Academy of Sciences* **117**, 68 (2020).
- [41] R. S. Markiewicz, S. Sahrakorpi, M. Lindroos, H. Lin, and A. Bansil, One-band tight-binding model parametrization of the high- T_c cuprates including the effect of k_z dispersion, *Phys. Rev. B* **72**, 054519 (2005).
- [42] S. C. Riggs, O. Vafek, J. B. Kemper, J. B. Betts, A. Migliori, F. F. Balakirev, W. N. Hardy, R. Liang, D. A. Bonn, and G. S. Boebinger, Heat capacity through the magnetic-field-induced resistive transition in an underdoped high-temperature superconductor, *Nature Physics* **7**, 332 (2011).
- [43] J. L. Tallon, J. W. Loram, J. R. Cooper, C. Panagopoulos, and C. Bernhard, Superfluid density in cuprate high- T_c superconductors: A new paradigm, *Phys. Rev. B* **68**, 180501 (2003).
- [44] A. Hosseini, D. M. Broun, D. E. Sheehy, T. P. Davis, M. Franz, W. N. Hardy, R. Liang, and D. A. Bonn, Survival of the d -wave superconducting state near the edge of antiferromagnetism in the cuprate phase diagram, *Phys. Rev. Lett.* **93**, 107003 (2004).
- [45] S. K. Yip and J. A. Sauls, Circular dichroism and birefringence in unconventional superconductors, *Journal of*

- Low Temperature Physics* **86**, 257 (1992).
- [46] Q. Li, Y. Tsay, M. Suenaga, G. Gu, and N. Koshizuka, Superconducting coupling along the c-axis of [001] twist grain-boundaries in $\text{Bi}_2\text{Sr}_2\text{CaCu}_2\text{O}_{8+\delta}$ bicrystals, *Physica C: Superconductivity* **282-287**, 1495 (1997).
- [47] Y. Zhu, M. Liao, Q. Zhang, F. Meng, R. Zhong, J. Schneeloch, G. Gu, L. Gu, X. Ma, D. Zhang, *et al.*, Isotropic josephson tunneling in c-axis twist bicrystals of $\text{Bi}_2\text{Sr}_2\text{CaCu}_2\text{O}_{8+\delta}$, arXiv preprint arXiv:1903.07965 (2019).
- [48] W. Harrison, *Electronic Structure and the Properties of Solids: The Physics of the Chemical Bond*, Dover Books on Physics (Dover Publications, 2012).
- [49] A. Bansil, M. Lindroos, S. Sahrakorpi, and R. Markiewicz, Influence of the third dimension of quasi-two-dimensional cuprate superconductors on angle-resolved photoemission spectra, *Physical Review B* **71**, 012503 (2005).
- [50] J. Slezak, J. Lee, M. Wang, K. McElroy, K. Fujita, B. Andersen, P. Hirschfeld, H. Eisaki, S. Uchida, and J. Davis, Imaging the impact on cuprate superconductivity of varying the interatomic distances within individual crystal unit cells, *Proceedings of the National Academy of Sciences* **105**, 3203 (2008).
- [51] P. Coleman, *Introduction to many-body physics* (Cambridge University Press, 2015).
- [52] B. A. Bernevig and T. L. Hughes, *Topological insulators and topological superconductors* (Princeton university press, 2013).
- [53] D. L. Feng, N. P. Armitage, D. H. Lu, A. Damascelli, J. P. Hu, P. Bogdanov, A. Lanzara, F. Ronning, K. M. Shen, H. Eisaki, C. Kim, Z.-X. Shen, J.-i. Shimoyama, and K. Kishio, Bilayer splitting in the electronic structure of heavily overdoped $\text{Bi}_2\text{Sr}_2\text{CaCu}_2\text{O}_{8+\delta}$, *Phys. Rev. Lett.* **86**, 5550 (2001).
- [54] T. Yokoyama, S. Kawabata, T. Kato, and Y. Tanaka, Theory of macroscopic quantum tunneling in high-t c-axis josephson junctions, *Physical Review B* **76**, 134501 (2007).
- [55] J. P. Perdew, K. Burke, and M. Ernzerhof, Generalized gradient approximation made simple, *Phys. Rev. Lett.* **77**, 3865 (1996).
- [56] S. Grimme, Semiempirical gga-type density functional constructed with a long-range dispersion correction, *Journal of Computational Chemistry* **27**, 1787 (2006), <https://onlinelibrary.wiley.com/doi/pdf/10.1002/jcc.20495>

METHODS

Microscopic derivation of GL coefficients

From the continuum BdG model, defined by the matrix Hamiltonian (10), it is possible to derive the corresponding GL theory by directly expanding the free energy \mathcal{F}_{BdG} given in Eq. (11) in the powers of the superconducting order parameters. This procedure is made feasible by the fact that explicit expressions for the two positive-energy eigenvalues of $h_{\mathbf{k}}$ can be obtained and are given by

$$E_{\mathbf{k}\alpha} = \sqrt{(\Delta_{\mathbf{k}1}^2 + \Delta_{\mathbf{k}2}^2)/2 + \xi_{\mathbf{k}}^2 + g^2 + (-)^{\alpha} D_{\mathbf{k}}} \quad (13)$$

where $D_{\mathbf{k}}^2 = (\Delta_{\mathbf{k}1}^2 - \Delta_{\mathbf{k}2}^2)^2/4 + g^2(\Delta_{\mathbf{k}1}^2 + \Delta_{\mathbf{k}2}^2 + 4\xi_{\mathbf{k}}^2) - 2g^2\Delta_{\mathbf{k}1}\Delta_{\mathbf{k}2}\cos\varphi$ and $\alpha = 1, 2$. We now express the two d-wave gap functions as

$$\Delta_{\mathbf{k}1} = \psi \cos(2\alpha_{\mathbf{k}}), \quad \Delta_{\mathbf{k}2} = \psi \cos(2\alpha_{\mathbf{k}} - 2\theta), \quad (14)$$

substitute into (13) and expand the free energy (11) in the powers of the order parameter amplitude ψ to fourth order. This expansion results in many terms and is best carried out with the help of Mathematica or similar software capable of symbolic manipulations.

We are primarily interested in terms governing the phase difference between the two layers, that is, coefficients B and C in the GL free energy (2). These can be isolated by focusing on terms containing powers of $\cos\varphi$. Coefficient B is thus found as a prefactor of $\psi^2 \cos\varphi$ in the above expansion and reads

$$B = \cos(2\theta)N_F \sum_{s=\pm} \int_0^{\epsilon_c} d\xi \frac{-\pi sg}{\xi|\xi - sg|} \frac{\tanh|\xi - sg|}{2k_B T} \quad (15)$$

In deriving this expression we replaced the crystal momentum sum using the usual prescription $\sum_{\mathbf{k}} \rightarrow N_F \int_{-\epsilon_c}^{\epsilon_c} d\xi \int_0^{2\pi} d\phi$ where $N_F = L^2 m / \hbar^2$ is the normal-state density of states at the Fermi level, L is the system size and the angular integral has been performed. The remaining integral over the energy variable cannot be completed in the closed form but one can show that the integrand $f_B(\xi)$ is *negative* for all values of ξ and thus the integral itself is also negative, as expected on physical grounds. This is illustrated in Fig. 5(a).

Coefficient C can likewise be identified as a prefactor of the $\psi^4 \cos 2\varphi$ term in the expansion and has the form $C = (2 + \cos 4\theta)I_C$. Here $I_C = N_F \int_0^{\epsilon_c} f_C(\xi) d\xi$ is the corresponding energy integral similar to Eq. (15). Its integrand $f_C(\xi)$ has a more complicated structure and for the sake of brevity we do not show it explicitly. Importantly $f_C(\xi)$ is *positive* for all ξ and, as anticipated in the main text, is approximately equal to the integrand of Eq. (15) squared, as shown in Fig. 5(b). We thus conclude that the continuum BdG model indeed supports the GL

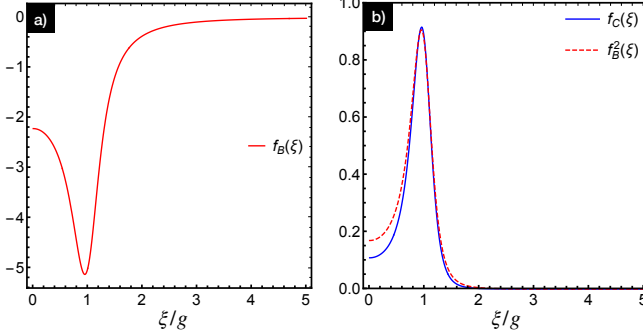


FIG. 5. Analysis of the energy integrands. (a) Integrand $f_B(\xi)$ entering the expression Eq. (15) for the GL theory coefficient B . (b) Integrand $f_C(\xi)$ entering the expression for the GL coefficient C compared to $f_B(\xi)^2$. Note that the amplitude of the latter is scaled by a constant factor of 1/30 for easier comparison. The temperature is chosen such that $k_B T = 0.2g$ but the qualitative properties of the integrands remain the same in a wide range of temperatures.

phenomenology deduced in the main text on the basis of general physical arguments. Specifically the calculation explicitly shows that prefactor \mathcal{K} of the $\cos 2\varphi$ term in Eq. (4) is positive which we argued was the key condition underlying the emergence of the \mathcal{T} -broken topological phase in the twisted dSC bilayers.

Self-consistent mean field theory on the lattice

To describe the two-layer system microscopically, we employ the Hubbard Hamiltonian (12) and treat the interaction term at the mean field level to account for d -wave superconductivity in each layer. The MF Hamiltonian becomes

$$H = -t \sum_{\langle ij \rangle \sigma a} c_{i\sigma a}^\dagger c_{j\sigma a} - t' \sum_{\langle\langle ij \rangle\rangle \sigma a} c_{i\sigma a}^\dagger c_{j\sigma a} - \mu \sum_{i\sigma a} n_{i\sigma a} + \sum_{\langle ij \rangle a} \left(\Delta_{ij,a} c_{i\uparrow a}^\dagger c_{j\downarrow a}^\dagger + \text{h.c.} \right) - \sum_{ij\sigma} g_{ij} c_{i\sigma 1}^\dagger c_{j\sigma 2}, \quad (16)$$

where t and t' are the hopping amplitudes between first and second neighbour sites on the square lattice, μ is the chemical potential that controls on-site particle density $n_{i\sigma a}$ and $\Delta_{ij,a} = V \langle c_{i\uparrow a} c_{j\downarrow a} \rangle$ is the complex order parameter. It is believed that the interlayer tunneling processes in cuprates are mediated, to leading order, by the spherically symmetric Cu 4s orbitals [S33], although other orbitals such as those belonging to Bi and Sr atoms, probably also play an important role. With this in mind, we adopt a phenomenological form for the interlayer tunneling amplitude that decays exponentially with distance:

$$g_{ij} = g_0 e^{-(r_{ij} - c)/\rho}, \quad (17)$$

where $r_{ij}^2 = c^2 + d_{ij}^2$, with d_{ij} denoting the in-plane separation between two sites i and j on different layers and c

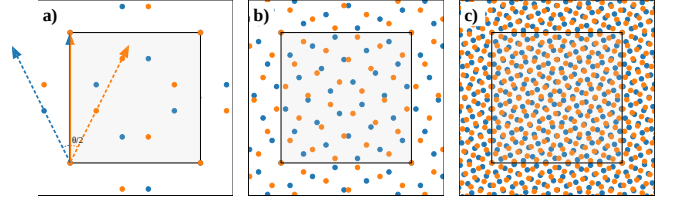


FIG. 6. Geometry of the commensurate unit cells for bilayers with relative twists of (a) $\theta_{1,2} \simeq 53.13^\circ$ (b) $\theta_{2,5} \simeq 43.60^\circ$ and (c) $\theta_{5,12} \simeq 45.24^\circ$. Twisting procedure is illustrated in panel (a) where orange and blue arrows indicate integer valued vectors $\mathbf{v} = (m, n)$ and $\bar{\mathbf{v}} = (-m, n)$ introduced in the text. Moire unit cell is shown by the shaded area.

being the interlayer distance. In practice, we limit these terms to a few unit cells, beyond which the amplitudes are negligible. The characteristic radial extent of the Cu 4s orbital has been denoted by ρ . We have also considered interlayer couplings of the form $g_{ij} = g_0 c^2 / r_{ij}^2$ [S48]. Self consistent calculations still result in topological phases, but this form of coupling, when compared to (17) for same g_0 , effectively corresponds to stronger interlayer coupling as the decay of $1/r^2$ is slower compared to the exponential.

While the above real space Hamiltonian is valid for any twist angle, the bilayer forms a crystal only for a discrete set of commensurate rotation angles. To carry out the lattice mean-field calculations we focus on commensurate twist geometries that are amenable to numerical study using the standard Bloch representation. We note that any commensurate twist can be described by an integer-valued ‘twist’ vector $\mathbf{v} = (m, n)$ as shown in Fig. 6. The corresponding moire unit cell comprises of $2q = 2(m^2 + n^2)$ sites and the twist angle is determined by the relation

$$\theta_{m,n} = 2 \arctan(m/n). \quad (18)$$

This can be understood as a rotation of two perfectly aligned square lattices in opposite directions by $\theta_{m,n}/2$, which leads to the sites originally at the locations \mathbf{v} and $\bar{\mathbf{v}} = (-m, n)$ to lie atop each other. The unit cells for a selection of commensurate twist angles close to 45° are illustrated in Fig. 6.

To model the Fermi surface of Bi2212 we follow Ref. [S24] and choose $t = 153$ meV, $t' = -0.45t$ with $\mu = -1.35t$ near optimal doping. Other parameters that determine the interlayer tunneling amplitudes are as follows: the average spatial extent of electrons in the 4s orbitals is $\rho \approx 4\text{a.u.} = 2.11\text{\AA}$, the typical inter-layer distance is $c \approx 12\text{\AA}$ [S49] and the in-plane separation between the Cu atoms is $a \approx 5.4\text{\AA}$ [S50].

In the remainder of this section we outline the procedure for obtaining gap equations for the order parameters $\Delta_{ij,a}$ using the imaginary time path integral formalism. After decoupling the attractive pairing potential in the Cooper channel with the Hubbard-Stratonovich transfor-

mentation, we obtain the action corresponding to the Hamiltonian (16) (cf. Ref. [S51] for details)

$$S = \sum_{\mathbf{k}n} \Psi_{\mathbf{k}n}^\dagger [-i\omega_n + h_{\mathbf{k}}] \Psi_{\mathbf{k}n} + \frac{\beta\mathcal{N}}{V} \sum_{\substack{i,j \in \text{u.c.} \\ a}} \Delta_{ij,a} \Delta_{ij,a}^*. \quad (19)$$

Here $h_{\mathbf{k}}$ is the BdG Hamiltonian that follows from Fourier transforming Eq. (16), $\beta = 1/k_B T$ is the inverse temperature, $\omega_n = (2n+1)\pi/\beta$ are the Matsubara frequencies, V is the strength of attractive nearest neighbour interactions, \mathcal{N} is the number of unit cells and $\Psi_{\mathbf{k}} = (\Phi_{\mathbf{k}1}, \Phi_{\mathbf{k}2})^T$ is the Nambu spinor such that $\Phi_{\mathbf{k}a} = (c_{\mathbf{k}\uparrow a}^{(1)}, \dots, c_{\mathbf{k}\uparrow a}^{(q)}, c_{-\mathbf{k}\downarrow a}^{(1)\dagger}, \dots, c_{-\mathbf{k}\downarrow a}^{(q)\dagger})^T$, with the superscripts $1, \dots, q$ labelling the sublattice degrees of freedom in layer a .

The effective action for $\Delta_{ij,a}$ can be determined by integrating out fermionic degrees of freedom

$$S_{\text{eff}} = - \sum_{\mathbf{k}n} \text{Tr} \log[-\mathcal{G}(\mathbf{k}, i\omega_n)^{-1}] + \frac{\beta\mathcal{N}}{V} \sum_{\substack{i,j \in \text{u.c.} \\ a}} \Delta_{ij,a} \Delta_{ij,a}^*, \quad (20)$$

where we defined the Matsubara Green's function $\mathcal{G}(\mathbf{k}, i\omega_n) = -(-i\omega_n + h_{\mathbf{k}})^{-1}$. To evaluate the saddle point condition for this effective action, $\partial S_{\text{eff}} / \partial \Delta_{ij,a}^* = 0$, we employ the identity $\partial_{\Delta}(\text{Tr} \log A) = \text{Tr}[\partial_{\Delta} A A^{-1}]$. After performing the Matsubara sum, this simplifies to

$$\Delta_{ij,a} = -\frac{V}{\mathcal{N}} \sum_{\mathbf{k}} \text{Tr} \left[\frac{\partial h_{\mathbf{k}}}{\partial \Delta_{ij,a}^*} U_{\mathbf{k}} n_F(E_{\mathbf{k}}) U_{\mathbf{k}}^\dagger \right]. \quad (21)$$

In the above, $U_{\mathbf{k}}$ is the unitary matrix that diagonalizes the Bloch Hamiltonian as $U_{\mathbf{k}}^\dagger h_{\mathbf{k}} U_{\mathbf{k}} = E_{\mathbf{k}}$ and $n_F(E_{\mathbf{k}})$ is a diagonal matrix where Fermi function is applied to the eigenvalues $E_{\mathbf{k}}$. For decoupled layers ($g_0 = 0$), with the tight binding parameters given above, a self-consistent solution converges to a d -wave form with maximal gap $\Delta_{\text{max}} = 40$ meV, when $V = 146$ meV. We use this value for calculations where two layers are coupled ($g_0 \neq 0$). Fig. 3 in the main text summarizes the results obtained from these calculations.

Topological phases

Here, we discuss in greater detail the various phases found in the self-consistent treatment of the lattice model.

To reliably determine the topology of the band structure, we turn to the Chern number, which is defined as an integral of the Berry curvature over the full Brillouin zone: $C = \frac{1}{2\pi} \int_{\text{BZ}} \Omega(\mathbf{k}) d^2k$. Computation of the Berry curvature directly from the eigenstates is complicated by the arbitrary phases that accompany numerical diagonalization. To counter this, we rely on a gauge independent

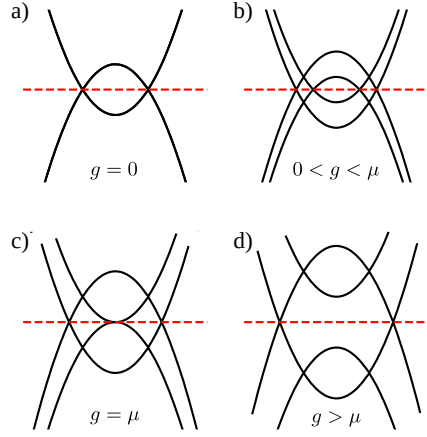


FIG. 7. Schematic picture for the normal state band structure of the continuum model defined in Eq. (7). Both electron and hole bands that enter the BdG Hamiltonian are shown while the Fermi level is indicated by a dashed red line. Panel (a) shows decoupled layers with doubly degenerate bands yielding a circular Fermi surface. In the presence of a d -wave order parameter we have eight Dirac cones. (b) Interlayer coupling g splits the bands and Fermi surface now consists of a pair of concentric circles. (c) The inner Fermi circle shrinks to a point and half of the Dirac cones disappear. (d) Four Dirac cones survive in the strong interlayer coupling ($g > \mu$) case.

formulation where [S52]

$$\Omega(\mathbf{k}) = \sum_{m \neq n} \frac{\langle n | \nabla_{\mathbf{k}} h_{\mathbf{k}} | m \rangle \times \langle m | \nabla_{\mathbf{k}} h_{\mathbf{k}} | n \rangle}{(E_m - E_n)^2}. \quad (22)$$

Here $|n\rangle$ and $|m\rangle$ are eigenstates of the Bloch Hamiltonian with energies E_n and E_m respectively.

The $C = \pm 4$ and ± 2 phases (indicated in Fig. 3(e) in red and green respectively) can be understood by considering the continuum model with a circular Fermi surface in the normal state, which we defined in Eq. (7). Similar arguments hold for the more realistic Fermi surface with hole pockets. When two layers are decoupled ($g = 0$), Fermi surfaces of each layer overlap, Fig. 7(a), and each layer hosts four Dirac cones in the presence of a $d_{x^2-y^2}$ order parameter. Upon breaking of \mathcal{T} , each Dirac point is gapped out and can contribute a Berry flux of $\pm\pi$, thereby allowing for the maximal value $C = \pm 4$. As we turn on the interlayer coupling, bands from each monolayer split, Fig. 7(b). If the interlayer coupling g is strong enough to push one of the bands above the Fermi level, half of the Dirac cones disappear, leaving four Dirac cones behind. In this case, the maximum Chern number is ± 2 , a situation realized in the phase diagram Fig. 3(e) for large g_0 .

It is interesting to note that the spectral gap tends to be larger in the $C = 2$ phase. We attribute this to

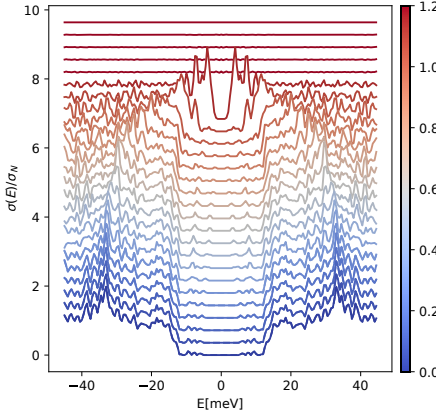


FIG. 8. Evolution of the density of states with temperature in the $C = 2$ phase with parameters $g_0 = 40$ meV and $\mu = -1.35t$. Temperature T/T_c shown as color scale. The superconducting gap persists up until $T = T_c$.

the fact that the $C = 2$ phase is stabilized at stronger values of the interlayer tunneling g_0 which enhances the Cooper pair tunneling amplitude. Moreover, in second order perturbation theory, the gap is expected to scale as g_0^2/Δ_0 . Temperature evolution of the corresponding tunneling density of states is shown in Fig. 8.

The gapped, topologically trivial $C = 0$ phase in the phase diagram can be understood as follows. As a representative of this phase, we consider the point $g_0 = 20$ meV and $\mu/t = -1.3$ for $\mathbf{v} = (1, 3)$ in the phase diagram Fig. 3(c). A self-consistent solution of the gap equation (21) yields the following forms for order parameters on the two layers

$$\Delta_{\mathbf{k}1} = \Delta_0(\cos k_x - e^{i\phi} \cos k_y) \quad (23)$$

$$\Delta_{\mathbf{k}2} = \Delta_0(\cos k_y - e^{i\phi} \cos k_x) \quad (24)$$

where Δ_1 and Δ_2 correspond to top and bottom layers respectively. The numerically obtained phase ϕ tends to be close to $-\pi/4$. If we define $\Delta^d = \Delta_0 e^{i\phi/2} \cos \phi/2$ and $\Delta^s = \Delta_0 e^{i\phi/2} \sin \phi/2$, order parameters can be cast as

$$\Delta_{\mathbf{k}1} = \Delta^d(\cos k_x - \cos k_y) - i\Delta^s(\cos k_x + \cos k_y)$$

$$\Delta_{\mathbf{k}2} = -\Delta^d(\cos k_x - \cos k_y) - i\Delta^s(\cos k_x + \cos k_y),$$

which shows that both layers have $d + is$ type superconducting order parameter. The transition between the $d + is$ and the $d + id'$ phases can be seen by tuning the chemical potential μ for a fixed interlayer coupling g_0 , as shown in Fig. 9.

Temperature dependence

The self-consistent gap equations can be also solved at non-zero temperature T . Although the Chern number is well defined only at $T = 0$ we may still compute

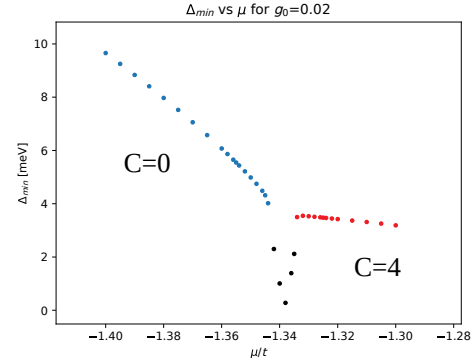


FIG. 9. The topological phase transition between $C = 0$ ($\mu < -1.34t$) and $C = 4$ ($\mu > -1.34t$) phases is marked by a closing of the gap as the chemical potential is tuned while keeping the interlayer coupling fixed at $g_0 = 20$ meV and $\theta_{2,5} \simeq 43.6^\circ$

C from Eq. (22) using the Bloch eigenstates obtained at $T > 0$. The resulting integer then describes the underlying mean-field band structure of the system at non-zero temperature. In this case, there will be no strictly quantized physical response (such as the thermal Hall conductance), but a nonzero C indicates the existence of protected chiral edge states that can be observed experimentally. In this sense the $T > 0$ phases with non-zero C can be regarded as topological and their properties related are to the $T = 0$ counterparts.

In Fig. 10 we compare phase diagrams at $T = T_c/2$ and $T = 0$. We observe that, remarkably, increasing temperature tends to suppress the topologically trivial $d + is$ phase in favor of topological $d + id'$ phases. Specifically at some points in the phase diagram increasing temperature can trigger a transition from the $d + is$ phase to the $d + id'$. This is illustrated in Fig. 10(c). As a result, we find that at elevated temperatures (but still well below T_c) essentially all of the phase diagram is taken over by the $C = 4$ and $C = 2$ topological phases.

Multiple CuO₂ planes

We now briefly discuss the extension of our theory to systems with $N > 1$ CuO₂ planes per monolayer, focusing on compounds with $N = 2$ such as Bi2212. The GL theory can be generalized by including complex order parameters χ_a describing the extra layers as illustrated in Fig. 11(a). For $N = 2$, the corresponding free energy density reads

$$\begin{aligned} \mathcal{F} = \mathcal{F}_0 + B(\psi_1 \psi_2^* + \text{c.c.}) + C(\psi_1^2 \psi_2^{*2} + \text{c.c.}) \\ + \sum_{a=1}^2 [B'(\psi_a \chi_a^* + \text{c.c.}) + C'(\psi_a^2 \chi_a^{*2} + \text{c.c.})], \end{aligned} \quad (25)$$

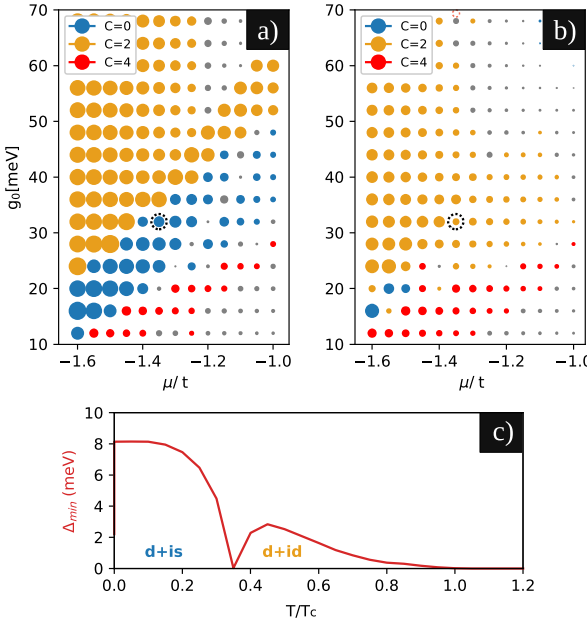


FIG. 10. Temperature dependence of the phase diagram is shown for $\theta_{2,5} \simeq 43.6^\circ$ at $T = 0$ and $T = T_c/2$ in panels (a) and (b) respectively. Panel (c) shows the minimum gap as a function of temperature for $g_0 = 32\text{meV}$ and $\mu = -1.35t$ (the parameters are indicated in panels (a) and (b) by a dashed circle)

where \mathcal{F}_0 collects all the terms that are independent of the relative phases between the layers and we only include coupling between adjacent layers. The most general ansatz for order parameters which respect the requisite symmetries would be

$$\begin{aligned} \psi_1 &= \psi e^{-i\varphi/2}, & \psi_2 &= \psi e^{i\varphi/2}, \\ \chi_1 &= \chi e^{-i\varphi'/2}, & \chi_2 &= \chi e^{i\varphi'/2}, \end{aligned} \quad (26)$$

with the amplitudes ψ and χ real and positive. The free energy (25) then becomes

$$\begin{aligned} \mathcal{F} &= \mathcal{F}_0 + 2B_0\psi^2 [-\cos(2\theta)\cos\varphi + \mathcal{K}\cos(2\varphi)] \\ &\quad + 2B'_0\psi\chi [-\cos(\delta\varphi) + \mathcal{K}'\cos(2\delta\varphi)], \end{aligned} \quad (27)$$

where $\delta\varphi = (\varphi - \varphi')/2$ and $\mathcal{K}' = C'\psi\chi/B'_0$. Observe that terms describing interlayer and intralayer phase differences, φ and $\delta\varphi$ respectively, can be minimized independently. The intralayer free energy, represented by the second line of Eq. (27), will be dominated by the single pair tunneling term $-\cos(\delta\varphi)$ on the account of the two CuO_2 planes being in a natural untwisted configuration. This implies $\delta\varphi = 0$: the two order parameters within each monolayer will be in phase, as expected. The remaining interlayer component of the free energy then coincides with Eq. (2) and its analysis proceeds exactly as before. This confirms that at the level of the GL theory, the presence of the extra layers has no effect on our prior conclusions.

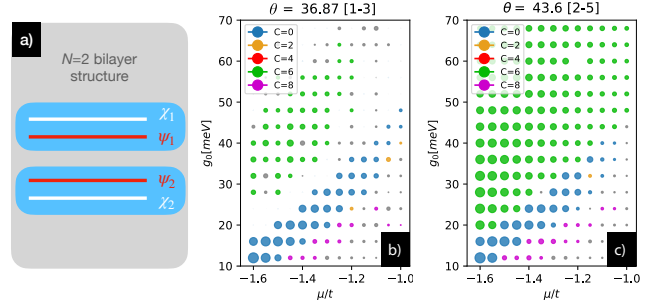


FIG. 11. Physics of systems with multiple CuO_2 planes per monolayer. a) The structure and notation used for the case with $N = 2$ CuO_2 planes. Panels b) and c) show phase diagrams of the lattice BdG model for bilayers with $N = 2$, relevant to the Bi2212 crystal structure with the intra-bilayer coupling set to $t_z = 40\text{meV}$.

Microscopic models can likewise be extended to the $N > 1$ case by adding appropriate CuO_2 planes to each monolayer. We illustrate this by considering a straightforward generalization of our lattice Hamiltonian Eq. (12) to $N = 2$. This is achieved by adding another square lattice of sites, which is described by the same Hamiltonian, to each monolayer and coupling the partner lattice sites by an intralayer tunneling term with amplitude t_z . Results of the $N = 2$ self-consistent calculation are shown in Fig. 11(b,c) where we chose $t_z = 40\text{meV}$ as appropriate for Bi2212 [S53]. We observe physics very similar to the $N = 1$ case, except that topological phases now exhibit Chern numbers 8 and 6, consistent with the notion that in the effective $d+id'$ state each CuO_2 plane contributes $C = 2$ to the aggregate Chern number of the system.

Josephson tunneling

In the past, several works have studied the problem of Cooper pair tunneling across c -axis twist junctions in order to understand the order parameter symmetry of cuprates [S24, S54]. Assuming a purely $d_{x^2-y^2}$ order parameter, it can be shown that the critical Josephson current must vanish when the twist angle is 45° . Recent experiments in twisted ultra-thin layers of Bi2212, however, observed that the critical current is essentially independent of the twist [S47]. Here, we show the current is indeed non-vanishing when \mathcal{T} is broken.

For the Josephson junction formed by the bilayer, the phase dependent supercurrent for a given c axis twist can be determined within the framework of the phenomenological GL theory via the relation

$$I(\varphi, \theta) = \frac{2e}{\hbar} \frac{\partial \mathcal{F}(\varphi, \theta)}{\partial \varphi}, \quad (28)$$

where the free energy has the form given in Eq. (4). A typical current-phase relation thus obtained is plotted in

Fig. 12(a). The critical Josephson current across the two layers for a given twist configuration, $I_c(\theta)$, may now be obtained by maximizing (28) with respect to φ .

As discussed in the main text, for twists in the vicinity of 45° , a $\mathcal{K} > 0$ ushers in a nonzero phase difference between the order parameters in the static case. This non-trivial character is manifest also in the behaviour of $I_c(\theta)$, as shown in Fig. 12(b). To elucidate this, we note that setting $\mathcal{K} = 0$ reproduces the behaviour of a junction formed by superconductors with pure d -wave character [S24, S54]. Note that $I_c(45^\circ) = 0$. For a positive \mathcal{K} , however, the critical current at 45° is non-vanishing. Given that rotations by θ and $\pi/2 - \theta$ are equivalent from the perspective of the bilayer, the functional form of the current respects this symmetry and so does its global maximum. The cusps at $\theta = 45^\circ$ can be seen as a consequence of this.

Density functional theory

We solved for the total energy of the twisted bilayer unit in DFT using the meta-GGA SCAN exchange

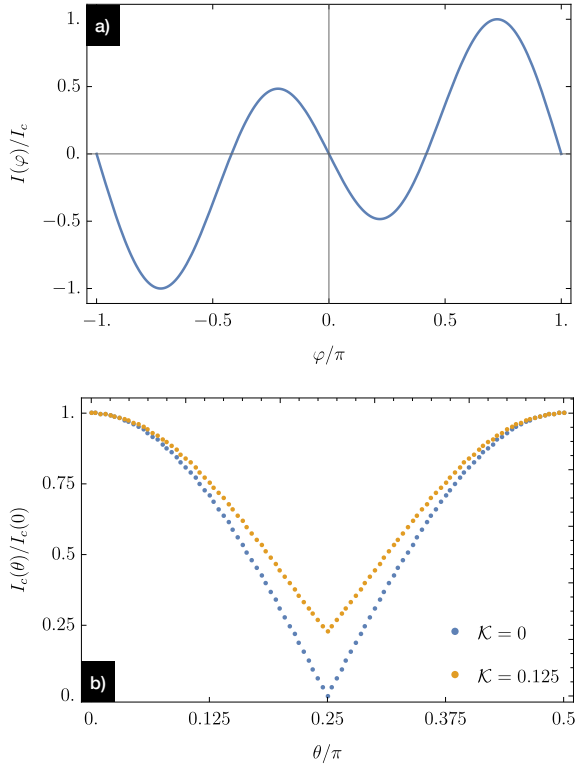


FIG. 12. (a) The current-phase relation in units of the critical current at twist $\theta = 41.4^\circ$ when $\mathcal{K} = 0.125$. (b) Twist angle dependence of the critical Josephson current normalized by the current in the untwisted case. While the two curves show similar behaviour close to $\theta = 0^\circ$ and 90° , a non-negative \mathcal{K} results in a finite value of the current at $\theta = 45^\circ$.

correlation potential [S36], as implemented in VASP [S37, S38]. Projector-Augmented-Wave pseudopotentials were used for the calculations. Results were converged for a plane-wave energy cutoff of 650 eV on a $(5 \times 5 \times 1)$ mesh. Similar results to those plotted in Fig. 4 of the main text were found in the generalized-gradient approximation [S55], with modestly increased optimal interlayer spacing. For the GGA calculations, we added Grimme's semi-empirical DFT-D2 approximation [S56] to better account for the long-range van der Waals binding between the bilayers.

In the main text, we made an effort to parameterize the interlayer coupling by evaluating the strength of hybridization between Cu 3d bands at the unfolded zone edge, or X point. This momentum point was chosen as previous studies of interlayer coupling in cuprates have indicated its vanishing strength along the ΓM line [S41]. The X point is then a suitable high-symmetry point where an interlayer-coupling driven hybridization may be studied. Despite the high density of bands, we have identified a suitable band splitting which is stable and monotonic over a sufficiently wide range of interlayer spacings, so that an approximate interlayer coupling evolution can be extracted. The results, for the unshifted-unit cell, are summarized in Fig. 4(d) of the main text, and reproduced in Fig. 13(b).

The recently developed SCAN meta-GGA presents the opportunity to perform DFT on this system without introducing the empirical vdW corrections required for standard GGA. It was developed with the intention of modelling mixed-bonding systems [S36]. SCAN has been successfully applied to calculations of both LSCO [S39] and YBCO [S40]. To confirm the reliability of our results, and their independence of the exchange-correlation potential, we compare the results of our interlayer coupling calculations, as computed using standard GGA (with the Grimme correction), against the SCAN meta-GGA. For simplicity, we use the unshifted unit cell of Fig. 4(b). A summary of the cohesive energy, as well as the interlayer coupling, is provided in Fig. 13. Both SCAN and the vdW-corrected GGA predict a total energy minimum at 12.87 Å, albeit with different cohesive energies. The similarities are even closer when comparing the X-point splitting, presented in Fig. 13(b). The splitting decays inversely with the Cu-Cu spacing, and the equilibrium splitting are nearly indistinguishable. The agreement between these results indicates the reliability of our X -point metric as an indicator of the interlayer coupling.

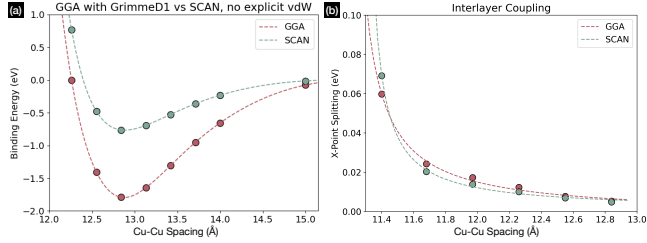


FIG. 13. Bilayer in Density Functional Theory: In panel (a), comparison of cohesive energy of twisted bilayer Bi2201, as computed in both the GGA and SCAN meta-GGA. Both exchange correlation potentials recover the same equilibrium spacing. (b) shows the X -point splitting, computed as in LDA described in the main text.